Astron. Astrophys. 358, 728–740 (2000)

ASTRONOMY AND ASTROPHYSICS

Multi-wavelength study of the slow "disparition brusque" of a filament observed with SOHO

B. Schmieder[1,2], **C. Delannée**[3], **Deng Yuan Yong**[4], **J.C. Vial**[5], **and M. Madjarska**[6,7]

[1] Observatoire de Paris – Section de Meudon, LPSH 2080, 92195 Meudon Principal Cedex, France (Schmieder@mesioa.obspm.fr)
[2] Institut of Astrophysics, University of Oslo, Blindern, Norway
[3] NASA/Goddard Space Flight Center, SOHO EAF, Code 682.3, Building 26, Room G-1, Greenbelt, Maryland 20771, USA
[4] Beijing Astronomical Observatory, National Astronomical Observatories, Chinese Academy of Sciences, Beijing 100012, P.R. China
[5] Institut d'Astrophysique Spatiale, Université Paris Sud, CNRS, bât. 121, 91405 Orsay, France
[6] Institute of Astronomy, 72 Tzarigradsko chausse Blvd., 1784, Sofia, Bulgaria
[7] Armagh Observatory, Armagh BT61 9DG, Ireland

Received 7 February 2000 / Accepted 29 February 2000

Abstract. A mid-latitude filament was observed before and after its eruption with SOHO (EIT, SUMER, CDS and LASCO) and with ground based observatories (Meudon and Pic du Midi) in the context of a coordinated MEDOC campaign in Orsay. The eruption was followed by a large Coronal Mass Ejection well observed by LASCO. Few hours before its eruption, the filament is partially heated (as seen in 195 Å with EIT). The physical conditions of the filament before its eruption have been investigated by spectroscopic analysis of SUMER (the Lyman series L4 to L9) and of CDS combined with the Multi-channel Subtractive Double Pass Spectrograph (MSDP) spectra of Hα. Five hours before the eruption, large broadenings of chromospheric and transition region lines (CDS) were observed in the main body of the filament suggesting strong turbulence as well as opposite Dopplershifts on each side of the filament (Hα and He I) which could be interpreted as twist motions. The optical thickness of the filament is rather large. During the eruption the twist is largely developed as observed in 304 Å. The Doppler shifts of the filament estimated from Lyman lines are in good agreement with the velocity of the front edge of the CME bright loop. We notice that both, the filament and the bright loop, are deviated towards the equator. This implies that they belong to the same global expansion event constrained to remain in the equatorial streamer. An X-ray bright point observed close to a filament footpoint could be the signature of reconnection process linked to the destabilization of the filament. It is interpreted in the framework of new MHD modeling of lateral filament footpoints (Aulanier & Démoulin 1998).

Key words: Sun: activity – Sun: chromosphere – Sun: corona – Sun: filaments

1. Introduction

"Disparitions brusques" were already observed by D'Azambuja (1948). This word defined the disappearance of a filament observed in Hα with spectroheliographs between two consecutive days.

They can be of thermal nature (Mouradian et al. 1986) or of dynamic nature (Démoulin & Vial 1992). In the latter case they are associated with catastrophic reconnection in the supporting magnetic field, destroying the prominence and leading to material ejection and acceleration of electrons in the high corona (Raadu et al. 1987). This disappearance of filaments is sometimes connected to other type of activity i.e. flares (Simon et al. 1984). The global magnetic structure surrounding the prominence and the amount of energy play important roles in the evolution of activated filaments. Moreover, the question arises: what does initially produce filament destabilization? And how does the filament react?

From SMM/UVSP observations coordinated with white light and Hα observations, Simon et al. (1986) related the filament activation to birth and motion of pores (small sunspots) close to the end of the disturbed section. They interpreted these pores as indications of new emerging flux. Raadu et al. (1988) proposed a sketch model where the new emerging flux could be associated to an active generation of currents by photospheric motions (Kuin & Martens 1988). This could increase the twisting (current) of the filament directly producing the observed rotational motion and also tending to destabilize it with respect to kink instabilities. A non linear development of the kink instability would restructure the magnetic field and may be the cause of upward motions and in favour of filament eruption.

An alternative explanation of the triggering mechanism may be provided in the context of some coronal reconnection (Antiochos et al. 1999).

The conditions of destabilization of filaments is still not well known. But nowadays we have a better understanding of the magnetic configuration of filaments. The recent 3D modelling developed by Aulanier & Démoulin (1998) shows that a filament can be represented by a twisted flux rope in a bipolar background and the parasitic polarities in the filament channel can be responsible for the existence of lateral footpoints. So we should be able to have a better insight to the problem of disap-

Send offprint requests to: B. Schmieder

pearance of filament: the triggering mechanism and the physical properties of the filament plasma. We have the opportunity to approach this problem by using recent multi-wavelength observations. SOHO with all its instruments on board, provides a large data set of a very spectacular eruption on May 31 1997 at 13:19 UT. LASCO observed until 19:49 UT the development of a very large Coronal Mass Ejection related to this eruption. We propose to study the time evolution of the prominence, the possible trigger mechanism involved and the physical conditions of the filaments through its eruption.

2. Observations

A quiescent filament located N 34 W 40 was observed on May 31 1997 before and during its eruption by ground-based and SOHO instruments in the context of a MEDOC campaign in Orsay following the Joint Observation Program (JOP17).

2.1. Ground-based instruments

In Meudon the spectroheliograph has a routine program and provides 5 full disk images per day (Hα, Ca II line center and in the 2 wings, an overexposed Ca II line center to detect the prominences). The heliograph provided one Hα image of full disk every minute between 06:00 UT and 14:00 UT.

Velocity and intensity maps in the Hα line were obtained with the Multi-Channel Subtractive Double Pass (MSDP) spectrograph (Mein 1991) at Pic du Midi. This instrument provides simultaneous data at nine spectral positions covering the Hα profile, with a field-of-view of $30'' \times 240''$. The Hα profiles were reconstructed for each pixel of the region. We got only one set of maps because of poor weather quality.

2.2. SOHO instruments

1. The prominence ejection is well observed by the Large Angle and Spectrometric Coronagraphs C1 and C2 (Brueckner et al. 1995) which detected the related CME from 12:07 UT to 19:49 UT. LASCO C1 field of view is from 1.1 to 3. $R_\odot$ with a pixel size of 3 arcsec. The images are obtained using a Fabry Perot at the wavelength 5303$\pm$0.63 Å in which a Fe XIV line is the principal emission. LASCO C2 field of view is from 2 to 6 $R_\odot$. The pixel size is 11.4 arc sec. The wavelength band pass is 5800$\pm$600 Å in which the Thompson scattered light on the free electrons is the principal emission detected.
2. The Extreme UV Imaging Telescope (EIT) provided images in He II and in Fe XII (Delaboudinière et al. 1995). The pixel size of the CCD is 2.62 arc sec in the full resolution mode. The table of the observations time according to the wavelength is presented in Table 1.
3. Spectra were obtained by the Coronal Diagnostics Spectrometer (CDS) (Harrison et al. 1995). The slit is moved to obtain an image ($240''$x$240''$) in 44 minutes, followed by three reduced field-of-view rasters ($120''$x$240''$) in 22 minutes from 06:30 UT to 08:30 UT. After a gap of 5 hours, we observe again the large field-of-view and the small field-of-view from 13:33 UT to 14:43 UT. Six lines are observed: O IV at 554.51 Å, Ne VI at 562.77 Å, He I at 584.33 Å, He II at 607.53 Å, Mg IX at 368.06 Å, O V at 629.75 Å. The spatial resolution is $2.0'' \times 1.68''$ (Table 1).
4. The SUMER spectrometer aboard SOHO is described by Wilhelm et al. (1997).
   Three periods of observations with different sets of lines were obtained. The following lines were observed according to the time period:
   - between 06:33 UT and 07:32 UT
     N V at 1238.82 Å, N V at 1242.8 Å, Si I at 1256.49 Å, Si II at 1260.42 Å, C I at 1266.42 Å. The filament and its transition region is not well identifiable.
   - between 8:17 UT and 11:28 UT
     The second set of observations of SUMER concerns the series of Hydrogen Lyman lines. 178 spectra are available with a time step of 63 sec. The following lines were observed: L-8 at 923.117 Å, L-7 at 926.113 Å, L-6 at 930.607 Å, S VI at 933.251 Å, L-5 at 937.657 Å, S VI at 944.354, L-4 at 949.598 Å. The Lyman lines present a strong central reversal at the location of the filament.
   - between 12:00 UT and 14:00 UT
     The observations were performed in the O IV (1399 Å) and Si IV (1402 Å) lines. The filament was in fact gone and nothing indicates the presence of a filament transition region.

   The data reduction has been performed: flatfield, destretching (technics of Moran). The spectra have been calibrated in wavelength using photospheric lines (CI and NI) and the

Table 1. EIT and CDS Observations (CDS includes six wavelengths: O IV 554.51 Å, Ne VI 562.77 Å, He I 584.33 Å, He II 607.53 Å, Mg IX 368.06 Å, O V 629.75 Å. Spectral resolution is 0.07 Å for Mg IX, and 0.12 Å for others)

	Time (UT)	Resolution	Field of View	
	01:18:39	$2''.62$	full-disk	
	07:18:39	$2''.62$	full-disk	
304 Å	10:16 - 12:06	$2''.62$	$587'' \times 587''$	$\sim$10min cadence
	13:18:39	$2''.62$	full-disk	
	19:32:34	$2''.62$	full-disk	
	00:11 - 06:45	$5''.24$	full-disk	$\sim$17min cadence
	01:12:46	$2''.62$	full-disk	
	07:12:45	$2''.62$	full-disk	
	09:00:34	$5''.24$	full-disk	
195 Å	10:57:24	$5''.24$	full-disk	
	13:12:46	$2''.62$	full-disk	
	13:26:41	$5''.24$	full-disk	
	18:53:28	$5''.24$	full-disk	
	19:26:39	$2''.62$	full-disk	
	19:44 - 23:54	$5''.24$	full-disk	$\sim$17min cadence
	06:33 - 07:19	$2''.03 \times 1''.68$	$240'' \times 240''$	
CDS	07:20 - 08:30	$2''.03 \times 1''.68$	$120'' \times 240''$	
	13:33 - 15:07	$2''.03 \times 1''.68$	$120'' \times 240''$	

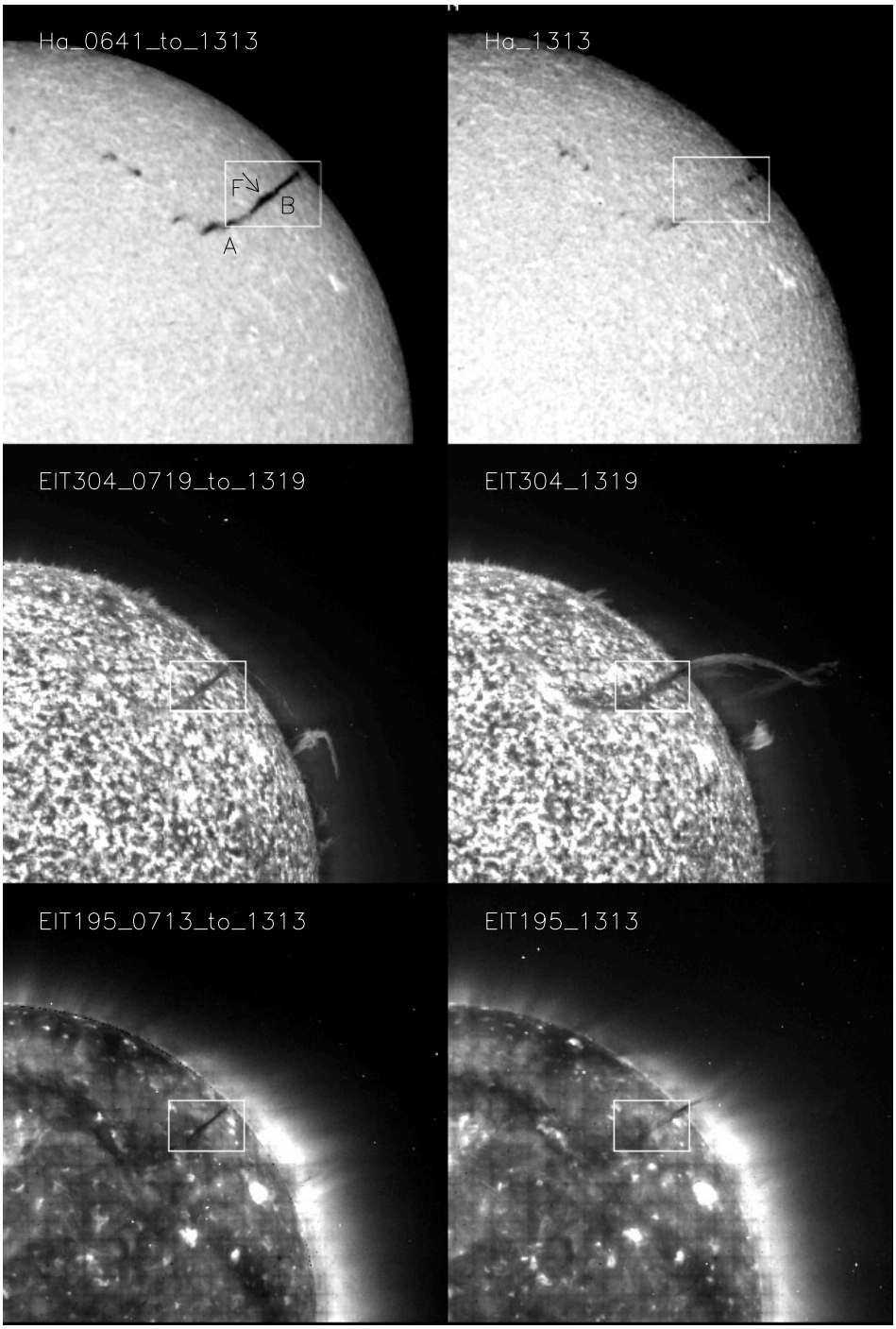

Fig. 1. Glance at the evolution of filament observed on May 31, 1997. From the upper to lower: Hα image from Meudon Spectroheliograph, SOHO EIT 304 Å, SOHO EIT 195 Å. The left panels have been rotated to the corresponding time of the right panels. Box denotes the region observed by MSDP (see Fig. 2). A and B in the Hα image indicate the two sections of the filament and F the footpoint between them.

software developed in Oslo and in intensity (using the radiometry procedure updated by Klaus Wilhelm).

3. Overview of the filament

In Fig. 1 are presented the filament observed in three different wavelengths corresponding to three different temperatures: Hα (10^4 K), 304 Å (8×10^4 K), 195 Å (1.6×10^6 K) before (around 07 UT) and during its eruption (13:15 UT). The images at 07 UT have been rotated to the time of the eruption. The filament channel points out the displacement of the filament plane toward the south. The plane seems to have been rotated by an angle of 10 degrees. This angle is well visible in the zoom images (Fig. 2) corresponding to the box of Fig. 1. This indicates a deviation of the filament towards the equator.

The filament consists in two sections A and B with a lateral northern footpoint F. The evolution of the two sections is different. From the heliograph survey we saw that the eastern A part gets diffuse around 10:50 UT and disappears completely around 12:00 UT, the western B part starts to be diffuse around 12:40 UT and is no more visible at 13:08 UT. A short macrospicule-

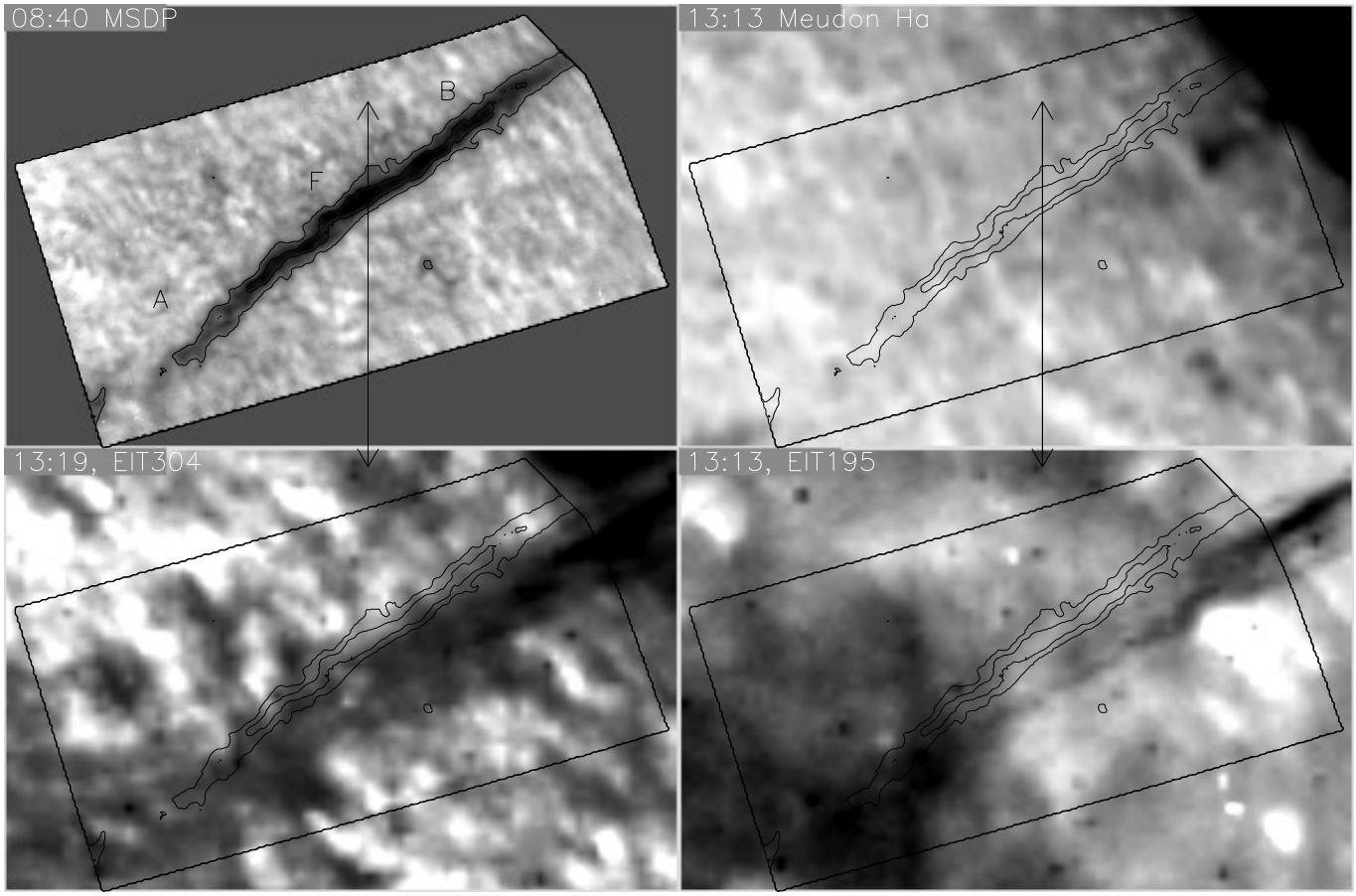

Fig. 2. The upper left panel is the Hα image of the line center from Pic du Midi Multi-channel Subtractive Double Pass (MSDP) spectrograph, A and B represent the 2 sections of the filament and F the footpoint between them; The upper right is Meudon spectroheliogram at 13:13UT; The lower two are EIT images; the arrow shows the position of SUMER slit at the 08:40 UT; Contour comes from Hα intensity (upper left). MSDP data were obtained at 08:40UT, but have been rotated to 13:13UT in this figure. FOV is about $219'' \times 146''$. Notice the rotation of the filament channel between 08:40 and 13:19 UT.

like prominence is visible at the limb in Hα from 09:08 UT to 14:03 UT. This section corresponds to the filament when it crosses the limb, viewed through its main axis.

3.1. UV and coronal filament observations

On the disk in 304 Å a large and long black area delineates the filament with lateral northern feet (Figs. 1 and 3). After 10:16 UT (notice the lack of 304 Å images between 07:18 UT and this time) part of the structure is observed as a prominence and the other part as a filament. Part A is better seen and the dark corridor extends towards the East as the time is progressing. That may be related to the extension and the rise of the lateral feet F (between A and B) with long fine structures connected to the surface. The eruption of the prominence is well visible at 304 Å as a long extended twisted tube (to 1/4 solar radius) at 13:19 UT.

The velocity of the prominence (11 km s^{-1}) in the disk plan can be estimated by measuring the shift of the top of the prominence from the 2 available images at 07:18 and 13:18 UT in 304 Å. It is certainly a low limit of the velocity because the prominence at 07:18 UT is a stable part of the filament when it crosses the limb as it is seen in Hα (see previous section). We have no real indication when the ejection starts on.

In 195 Å a thin dark thread lies in the filament channel, particularly along the section B. It is well visible at 06:45 UT (Fig. 3). It progressively moves towards the limb. The estimated velocity of progression toward the limb of the dark thread is between 2- 5 km s^{-1}. So, the motion of the dark thread likely results from a projection angle effect as the filament rotates with the sun. The apparent motion of the dark thread in the filament core at the time of the ejection is very slow compared to the prominence velocity. At 13:12 UT, only the prominence base is visible in dark (Fig. 4). Dark threads in 195 Å are the signature of absorption of the coronal line by cool plasma. In the prominence there is competition between absorption by cool plasma and emission by hot one. A possible interpretation of the difference is that the dark part of the filament is disappearing during the ejection because of the heating of the material: the material begins to emit in 195 Å as observed in the prominence part and the filament core tends to be less dark on the disk.

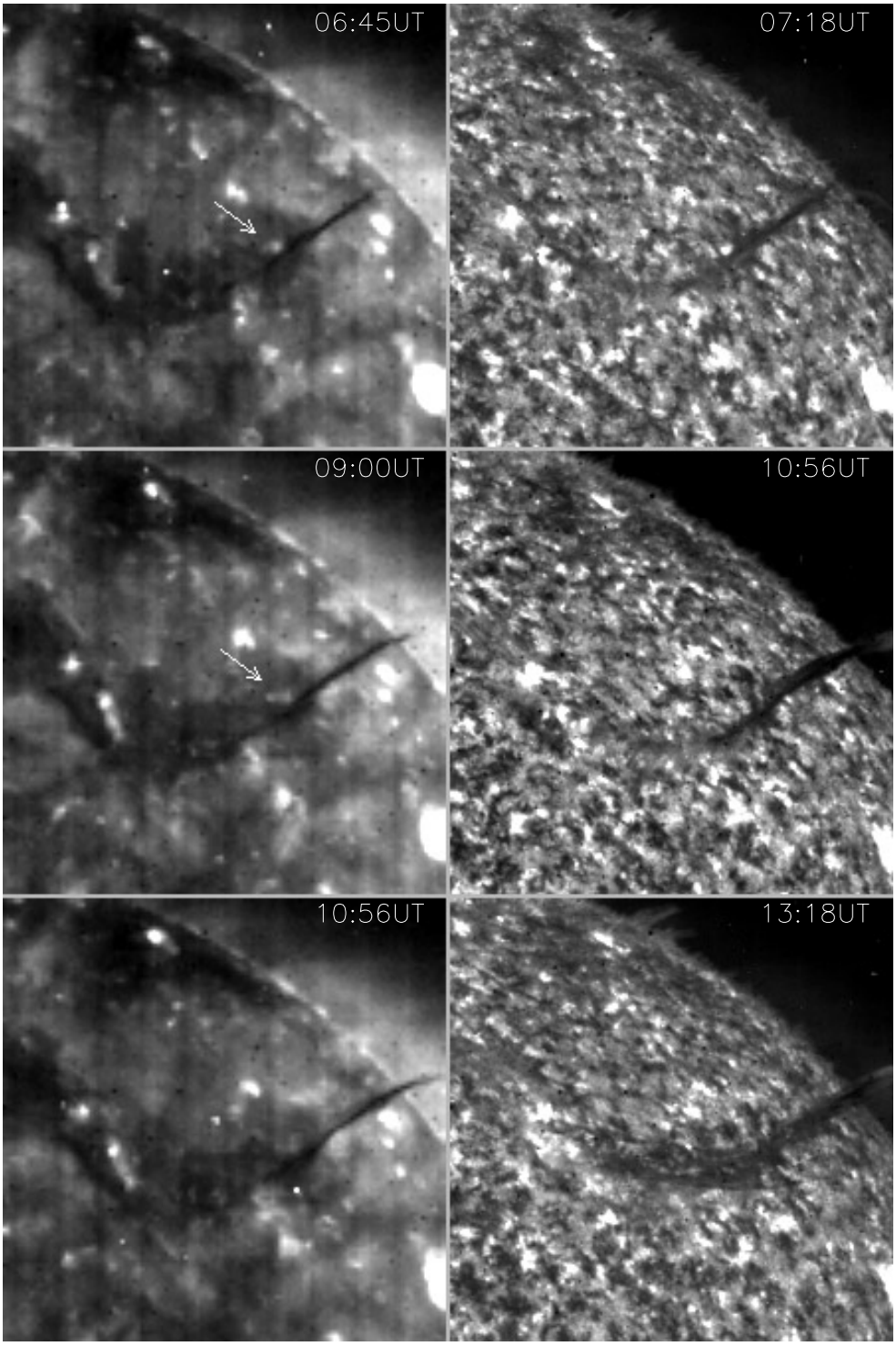

Fig. 3. Evolution of EIT 195 Å (left panels) and 304 Å (right panels). The bright point mentioned in the text is indicated by arrows in EIT 195 Å images. It could correspond to the site of a new emerging flux leading to reconnection and release of energy. Such phenomena could be the trigger of the filament destabilization.

A weak emission in 195 Å is observed above the limb in the prominence part with some structures showing the same shape as the 304 Å prominence (loop and crossing point in Fig. 4).

It is very difficult to observe flows in the filament core due to the poor spatial (5.24 arcsec) and temporal (17 min) resolution before the ejection. At the time of the ejection the images were mainly obtained with the 2.62 arcsec resolution but every hours in average.

3.2. Bright point

In 195 Å images (close to the footpoint F of the filament between section A and B in Fig. 3) we see the enhancement of a bright point (BP) between 06:45 UT and 09:00 UT. Because of the location of the BP close to F and the time coincidence with the beginning of the rise of the footpoint fine structures we suggest that the BP is related to the triggering of the destabilization

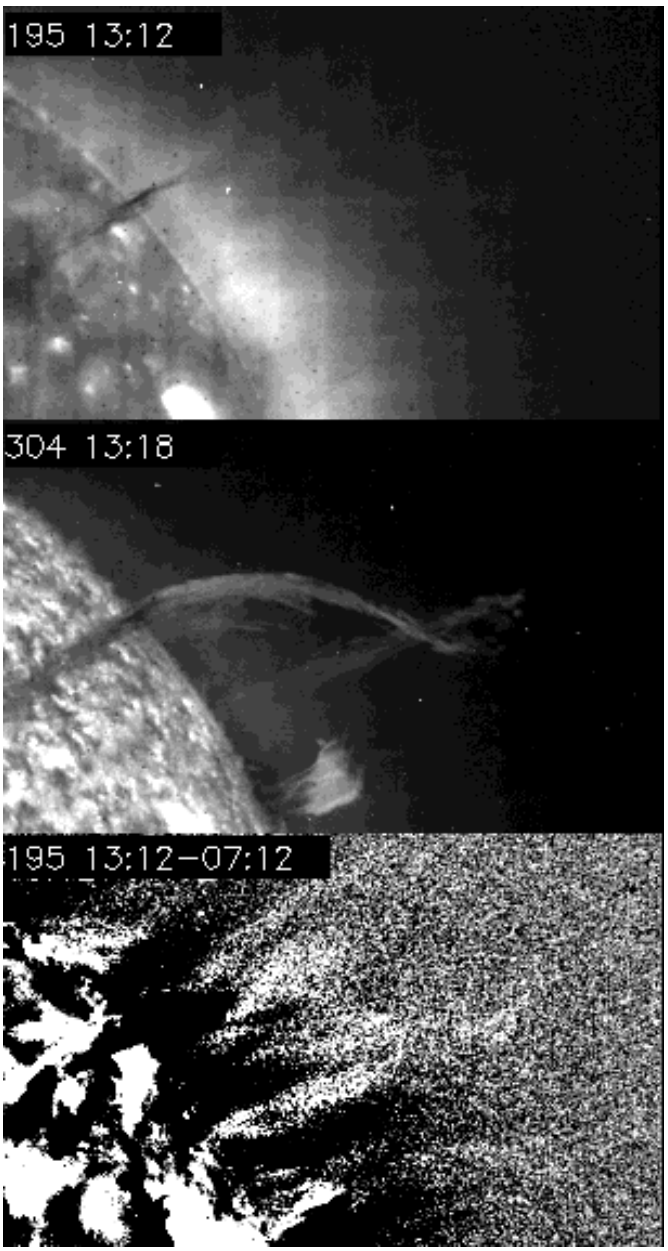

Fig. 4. EIT images of the prominence ejection in 195 Å at 13:12 UT, in 304 Å at 13:18 UT and the difference of the images obtained in 195 Å at 13:12 UT and at 7:12 UT. A part of the prominence is observed in absorption in 304 Å and a part of the prominence located in the small loop formed at its upper part is observed in emission in 195 Å (highligthened by the difference of images, emphasizing the low level signal and saturating the high level signal).

of the filament. The BP could be due to emergence of a new dipole and to reconnection processes. The location of the filament close to the limb did not allow to use MDI magnetograms to check this possibility. Brightening observed close to a footpoint had already been interpreted as the trigger of eruption and had been related to the observations of new emerging and fast moving polarities (Simon et al. 1984). The new field lines could reconnect with preexisting ones and the BP could be the signature of heating during the reconnection. Such idea has now a good support with the recent development o f the 3-D MHD modelling of filaments (Aulanier & Démoulin 1998, Aulanier et al. 1999). This model is based on the existence of a magnetic flux rope in a bipolar configuration. The lateral footpoints are explained by the presence of parasitic polarities in the filament channel which create new connectivities. The material of the footpoints are in the dips of these field lines. The emergence of a new pore close to these field lines could easily develop a destabilization of the filament. It can concern only one arch or section of the filament.

3.3. CME

The LASCO C1 images shows the emergence of a dark and bright feature above the NW limb after 12:07 UT (Fig. 5). A bright thin loop (marked at the head of the arrow in Fig. 5) appears above a cavity. The bright loop inflates until it escapes from the LASCO C1 field of view. The bright loop then appears in LASCO C2 field-of-view (Fig. 6). The bright loop is deviated toward the equator and force to be guided by the equatorial streamer field lines. This deviation towards the equator had already been mentioned in the filament overview (Sect. 3). The radial velocity is about 60 km s^{-1} in the LASCO C2 field-of-view. At the southern edge of the bright loop in the LASCO C1 field-of-view, a strong brightening appears. This brightening could correspond to a strong compression occurring at the feet of perturbed field lines as they inflate. A detailed analyzis of this kind of brightnings was done by Delannée & Aulanier (2000) and Delannée (2000). The overlay of the 304 Å EIT image at 13:18 UT with the LASCO C1 image at 13:28 UT (Fig. 7) shows that the prominence presents a strong Fe XIV emission in its upper part and at its outer border. The prominence in Fe XIV is thicker than in He II which again shows the heating of the prominence. The CME observed in the LASCO C2 image (Fig. 6) presents a twisted structure signature as it was already observed in other cases (Wood et al., 1999, Dere et al., 1999).

4. Physical parameters of the filament

4.1. Microturbulence and twist before the eruption

The MSDP profiles of each pixel of the filament are available at 08:40 UT few hours before the eruption (it is the only time available). The Hα profiles are relatively large in section B. This line broadening could correspond to high microturbulence or unresolved motions suggesting twist motions of the filament structures (Fig. 8).

In the Doppler shift map no large Doppler shifts were observed at this time (v= $\pm$ 2 km s^{-1}). Doppler shift fine structures in the main body of the filament (section B) are aligned along the main axis of the filament with blue shift in the south and red shift in the north (visible in the profiles shown in Fig. 8). Such a behaviour of the velocity field could be interpreted as twisted motions of filament fine structures as in previous studies (Schmieder et al. 1985; Simon et al. 1984).

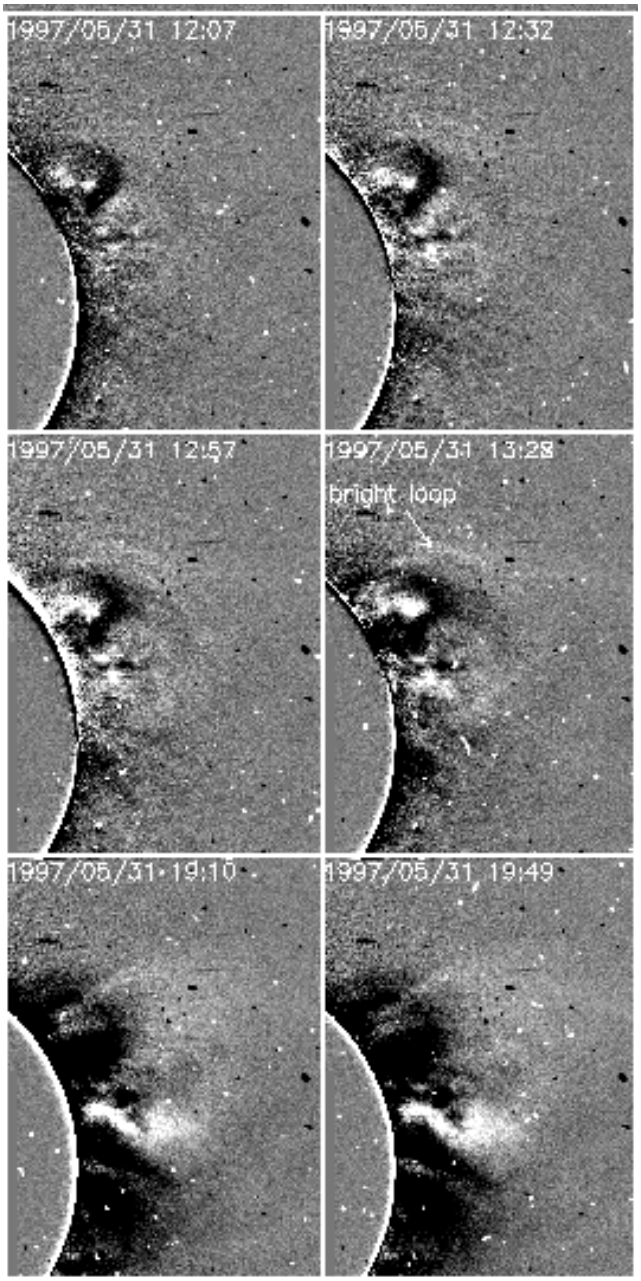

Fig. 5. LASCO C1 images of the ejection obtained in Fe XIV from 12:07 UT to 19:49 UT. Images are differences with an image obtained at 10:43 UT. A bright loop is formed above the prominence and moving outwards. One of its footpoint is located near the equator. It brightnens as the ejection occurs. The bright loop is visible as an open feature on the image at 19:49 UT.

The co-alignment of the Hα images with EIT and with CDS is presented in Figs. 2 and 9. The CDS 554 Å image is comparable to EIT 304 Å and represents the transition zone, the CDS 368 Å image looks like the EIT 195 Å image and is the signature of coronal temperature emission. EIT has a better time resolution but the spatial resolution of CDS is better than the EIT one. The field-of-view of CDS covers a part of sections A and B of the filament.

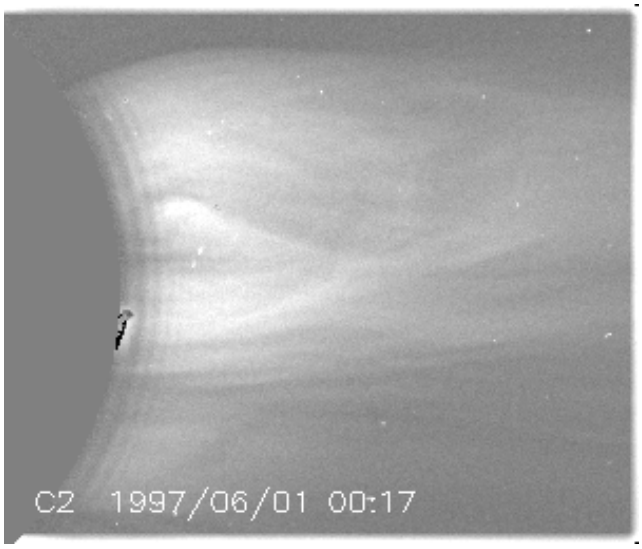

Fig. 6. White light image from LASCO C2 of the CME related to the prominence ejection. The CME presents signature of a twisted flux tube. The velocity is about 60 km s^{-1}.

CDS line profiles allow to compute the 3 moments: intensity, Dopplershift and line broadening. The transition region lines show a large broadening in the filament channel. Using He I and OV lines we derive Doppler shifts in the filament (Fig. 10). Due to the location of the filament close to the limb they represent mainly the horizontal component of the flows along the filament. Between 07:00 to 08:30 UT (after that time we have no CDS data) we see mainly red shift on the northern side of the filament and blue shift on the southern side. That could confirm the existence of a twist prior the eruption. The twist is well visible in section B. At the footpoint F no particular Doppler shift is observed around 08:30 UT. It is also what is noticed in Lyman lines.

The SUMER slit cuts the filament near its footpoint F according to the co-alignment between CDS and SUMER (Fig. 2). The Lyman lines observed in the filament over the disk show a central reversal. The central part corresponds to absorption by the cool filament plasma as it was already mentioned in the study of an other filament by Schmieder et al. (1998) (Fig. 12).

They are quite symmetrical and did not show such strong broadening. This can be explained easily. The Lyman lines are less sensitive to microturbulence because of their optical thickness compared with transition lines and because of their short wavelength compared with Hα wavelength nearly by a factor 6.

Before its eruption the filament is less and less visible in Hα due to partial heating (visible in 195 Å EIT images) and twisted (observed in 304 Å and suggested in Hα and He I) during few hours. Strong microturbulence is observed in the main body of the filament.

4.2. Bulk flows during the eruption

Only in some time periods we observe asymmetric profiles of the Lyman lines between 09:20 UT and 09:40 UT and again

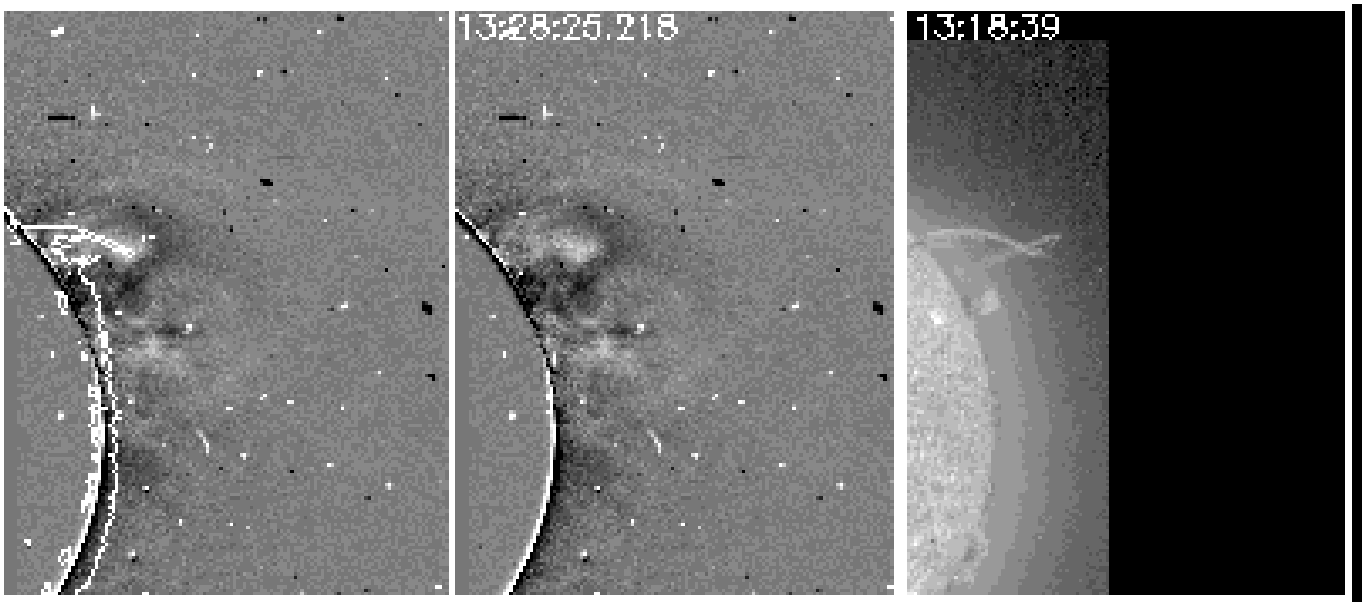

Fig. 7. Overlay of the 304 Å EIT image at 13:18 UT with the Fe XIV C1 image at 13:28 UT. The contours of the prominence in 304 Å are drawn on the first image over the Fe XIV C1 image. The C1 image is displayed on the second image and the 304 Å image on the third image. The brightest parts in the C1 image correspond to the upper part of the prominence.

Table 2. Flows in the filament versus time

Time UT	line	Instrument	Doppler shift in B ($km\,s^{-1}$)	Doppler shift footpoint ($km\,s^{-1}$)	Velocity ($km\,s^{-1}$)
06:30-8:30	He I, OV	CDS	twist	few	
08:40	Hα	MSDP	twist	few	
08:17-10:00	Lyman	SUMER	no data	few	
11:10-11:28	Lyman	SUMER	no data	~ 75	
07:18-13:18		EIT			$>$10 (prominence)
12:07-13:28		C2			60 (bright loop)

more clearly at the end of the sequence between 11:10 UT and 11:28 UT in an extended portion along the slit (Fig. 13). The blue peaks of the lines are weak. In a previous paper (Schmieder et al. 1998) we have shown that such asymmetry could be explained by high velocities of the cool material. The missing blue peak would indicate a strong blue shift of the filament. We can give an upper limit of such a velocity. A displacement of 0.25 Å corresponds to 75 $km\,s^{-1}$. In order to get accurate values of velocities a complete NLTE treatment is suitable. These Doppler shifts could correspond to horizontal velocities. Due to the position of the slit crossing a footpoint of the filament and the fact that at 11:00 UT we see mainly fine stretched structures in EIT images we think that such a geometry implies that the blueshift corresponds to the rise velocity of the threads of the lateral footpoint (Fig. 3). The threads are in a plane perpendicular to the solar surface and containing the line-of-sight.

The profiles in S VI observed simultaneously with Lyman lines are not shifted. They correspond to the transition zone but not to the filament.

The eruption starts with the rise of one footpoint stretching the prominence fine structures. The Doppler shifts estimated from Lyman lines (SUMER) are of the same order as the velocity of the bright loop of the CME (LASCO C2) (Table 2). That confirms the strong relationship between the prominence eruption and the CME.

4.3. Optical thickness and gas pressure

The Hα profiles of section B observed at 08:40 UT before the eruption are relatively broad. Line broadening could correspond to high microturbulence or unresolved motions as it was already mentioned. By analysing the profiles of Hα and using a cloud model method we can derive four parameters: the optical thickness of the filament τ, the source function S, the Doppler width and Doppler shifts (Fig. 8). There is a close correlation between the depth variation of the source function and the total optical thickness in the Hα line (Mein et al. 1996). In order to get the optical thickness we assume a constant source function taken at $\tau_0 \sim 1$. With a source function equal to half of the minimum of intensity of the Hα reference profile (I_{min}), we compute a τ value in the filament at the line center of the order of 2 to 3.

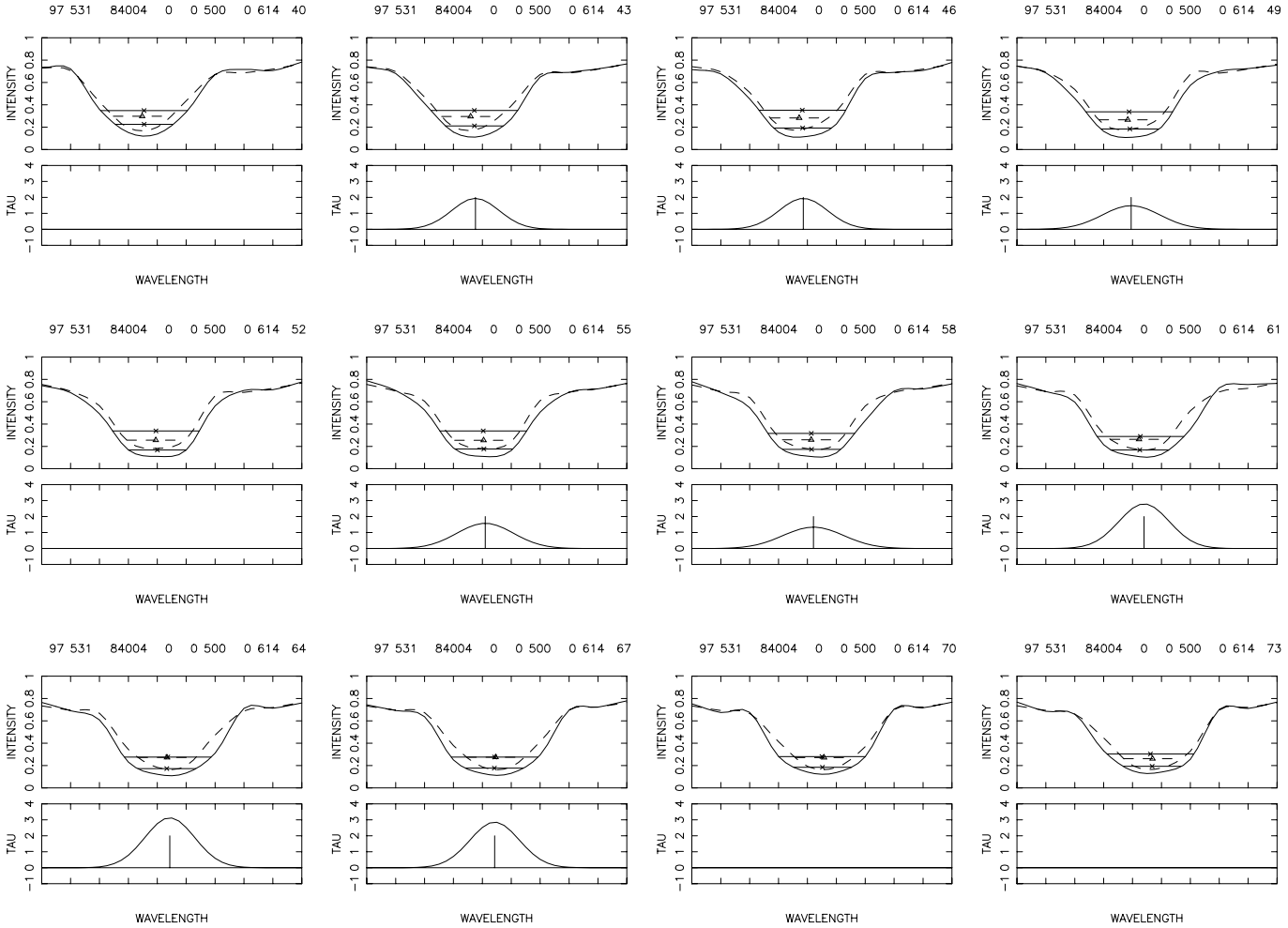

Fig. 8. Example of Hα profile (MSDP) through a cross-section of the B part of the filament. The left top profiles are mainly redshifted and correspond to the northern edge of the filament, the right bottom profiles are blueshifted and correspond to the southern edge. The middle row profiles are broadened profiles in the central part. Dashed profiles are reference chromospheric profiles. Continuous lines correspond to filament profiles. The low panels are τ profiles derived by the cloud model method.

Table 3. Intensity of Lyman lines in W $m^{-2}\,sr^{-1}A^{-1}$. Mean ratio of peak to center intensity. Ib (Ir): mean peak intensity of blue (red) wing; I0: mean center intensity; Im=(Ib+Ir)/2. Two time periods are calculated. For each line, the first row is the result of the first period, 08:37-09:24 UT, the second row corresponds to 10:32-11:19 UT

Line	Ib	Ir	I0	Ib/I0	Ir/I0	Im/I0
L-4	0.075	0.099	0.045	1.67	2.20	1.93
	0.12	0.10	0.083	1.46	1.24	1.35
L-5	0.049	0.059	0.037	1.33	1.61	1.47
	0.066	0.071	0.054	1.22	1.31	1.27
L-6	0.035	0.040	0.028	1.24	1.44	1.34
	0.038	0.054	0.031	1.22	1.70	1.46
L-7	0.025	0.030	0.019	1.29	1.53	1.41
	0.029	0.039	0.022	1.32	1.76	1.53
L-8	0.026	0.033	0.019	1.33	1.72	1.53
	0.043	0.037	0.030	1.43	1.22	1.32

It is important to see if this value is consistent with our Lyman lines results and their NLTE interpretation. The Lyman lines observed in the filament over the disk show a strong central reversal as it was already mentioned. The central part corresponds to absorption by the cool filament plasma (Fig. 12). Table 3 gives the main characteristics of the Lyman profiles. Before the eruption, the profiles are symmetric and comparable to line profiles observed previously in another filament (Schmieder et al. 1998). According to this previous paper, they could be fitted by NLTE modelization (GHV 1993) using a slab of D=20 000 km, T=7000 K, v = 5 km s^{-1} and with a pressure of p=0.1 dyn cm^{-2}.

In this 1 D model the total optical thickness τ_t(Hα) is around 20 (P. Heinzel, private communication). This value of τ_t(Hα) is large compared with the τ that we have determined with the constant source-function cloud model using the Hα profiles. We can conclude that either the NLTE model should be revised to fit exactly our present Lyman line profiles or the assumption of a constant source-function is not valid. Let us discuss the sen-

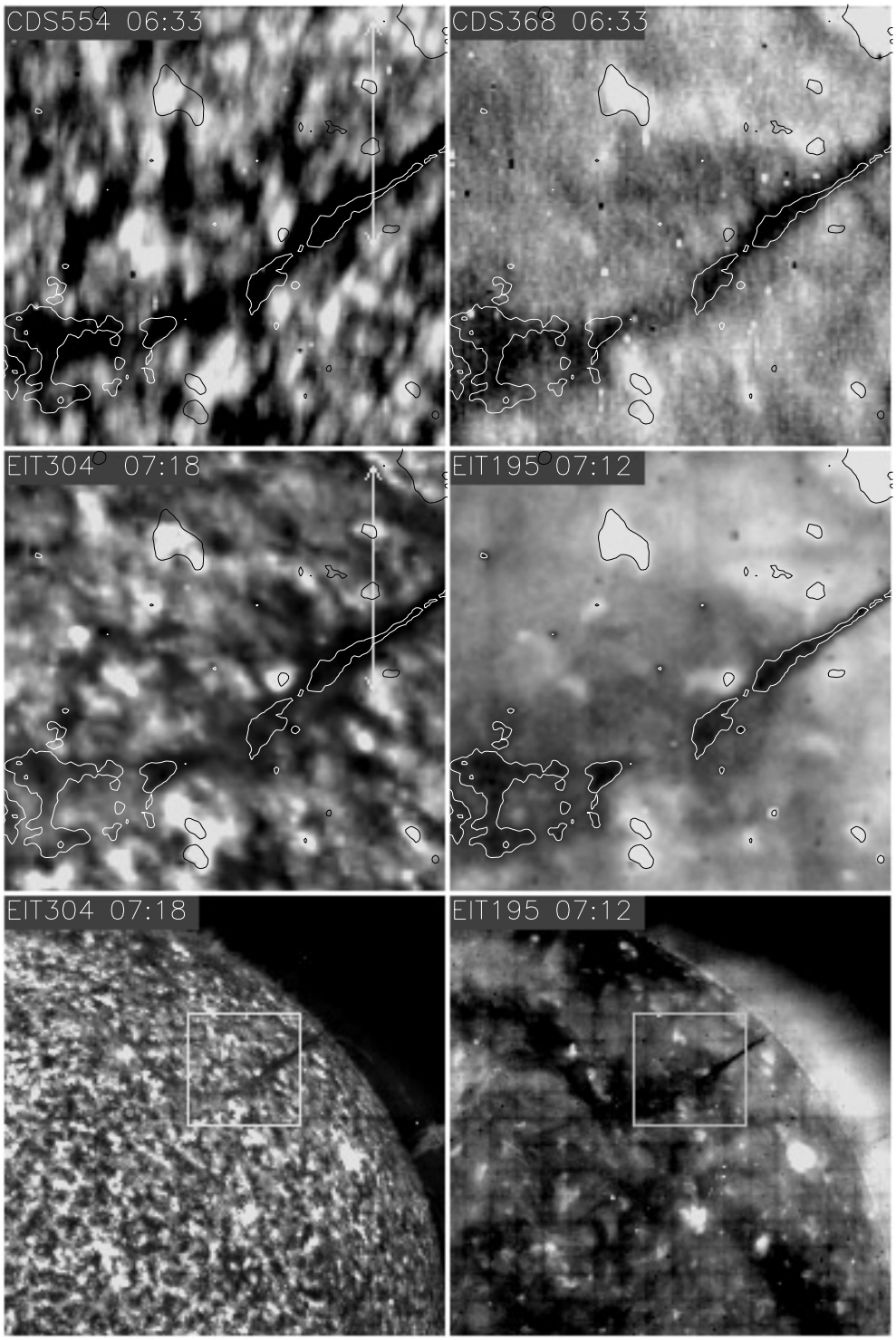

Fig. 9. Upper left: SOHO CDS OIV at 554.51 Å (06:33UT); upper right: SOHO CDS MgIX at 368.06 Å (06:33UT); Middle left: SOHO EIT 304 Å (07:18UT); Middle right: SOHO EIT 195 Å (07:12UT). FOV of CDS is about $240'' \times 240''$, its position on the disc is marked with box in the EIT images of lower panel. Contours in upper and middle panels come from EIT 195 Å of the middle right panel. Arrows correspond the position of SOHO SUMER slit (with some uncertainty).

sitivity of this latter assumption to our results. The considered source-function (S) normalized by the continuum at disk center is $\sim 5.5\%$. According to the curves $S(\tau)$ presented in Mein et al. (1996), it appears that many curves can fit with such a source-function at τ_0 =1 and lead to a $\tau_t(H\alpha)$ thickness around 10 to 20. The considered gas pressure is of the order of 0.1 dyn cm^{-2} or even larger and such a value is consistent with the Hα opacity and the Lyman line profiles reversals.

5. Conclusion

We have observed a long quiescent filament during its disk passage and its eruption on May 31, 1997. It was the target of the Joint Observation Program (JOP17) during a MEDOC campaign in Orsay. We concentrated our study on the pre-eruptive stage of the filament, the trigger mechanism leading to its destabilization and the eruption by using multi-wavelength observa-

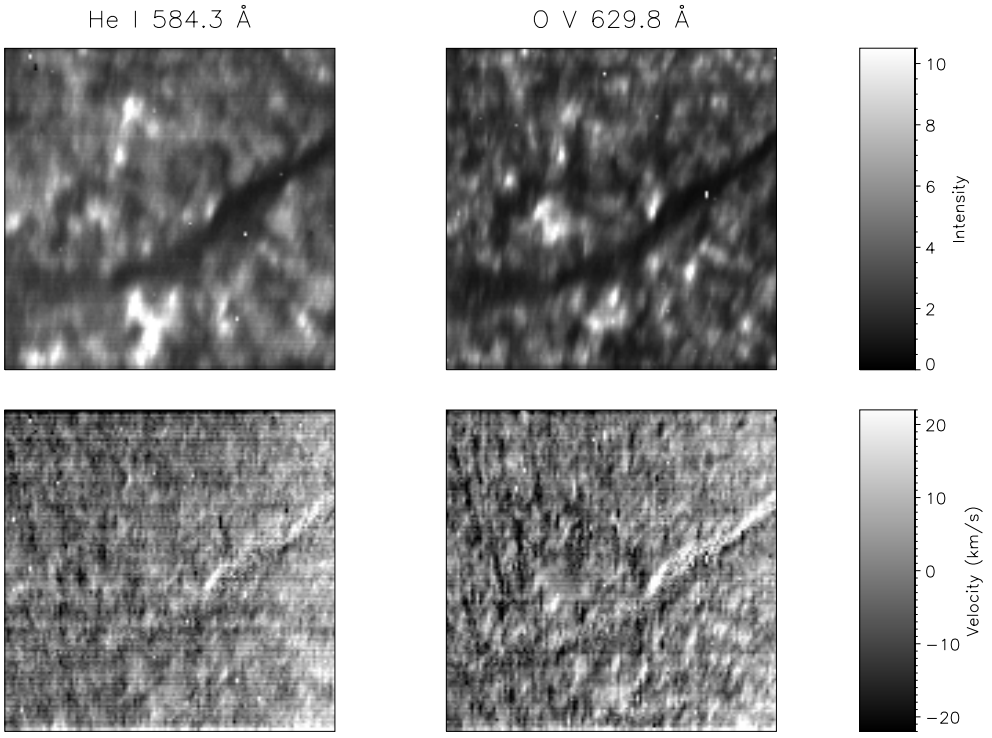

Fig. 10. CDS intensity and velocity in He I and O V lines between 06:33 and 07:19 UT. Note the red shift in the north and the blue shift in the south inside the filament channel.

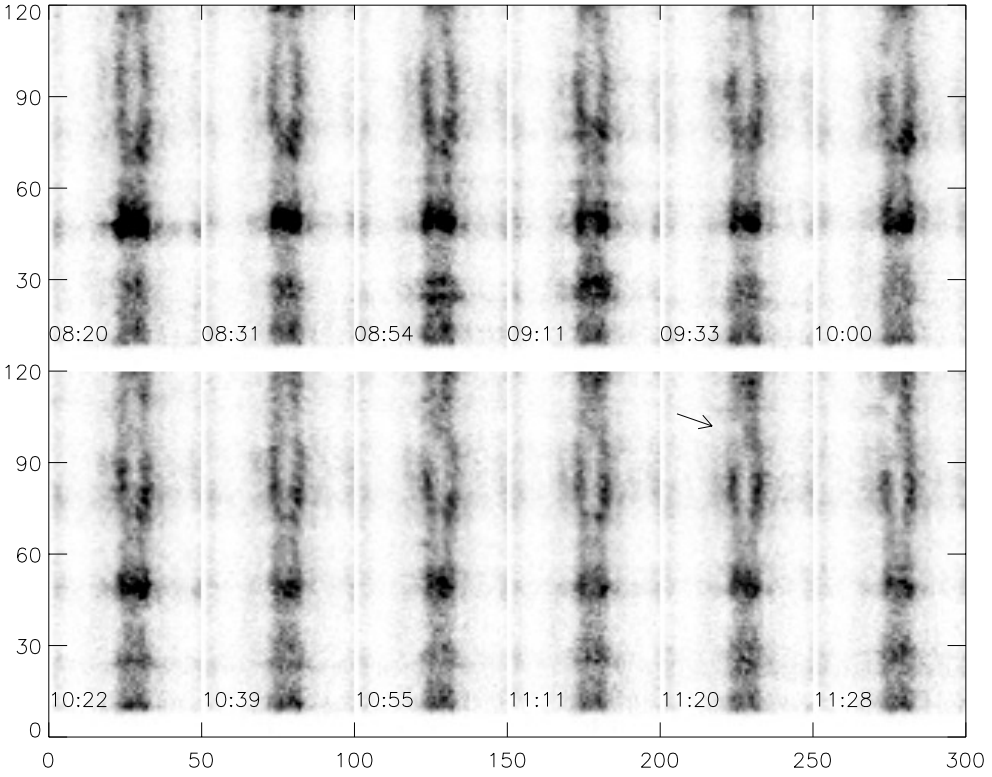

Fig. 11. Evolution of filament occurring in Lyman line L4 at selected times. The L4 line shows 2 peaks when the slit crosses the filament. The arrow indicates a region where the blue peak is missing.

tions obtained with ground-based and SOHO instruments (EIT, LASCO, CDS, SUMER). The filament consists of two main parts A and B. An X-ray bright point was detected in EIT 195 Å image near the footpoint F between A and B at 09:00 UT. Consequently we observe the slow di sappearance of section A in Hα due to heating process until 12 UT while the section B was deeply disturbed by microturbulence and twisted motions. The twisted motions are clearly seen in 304 Å and suggested in Hα and HeI Doppler shift maps at 08:40 UT by the existence of aligned regions of blue and redshifts along the filament axis. Such twisting motions have been described already in a disturbed Hα filament (Schmieder et al. 1985). These obser-

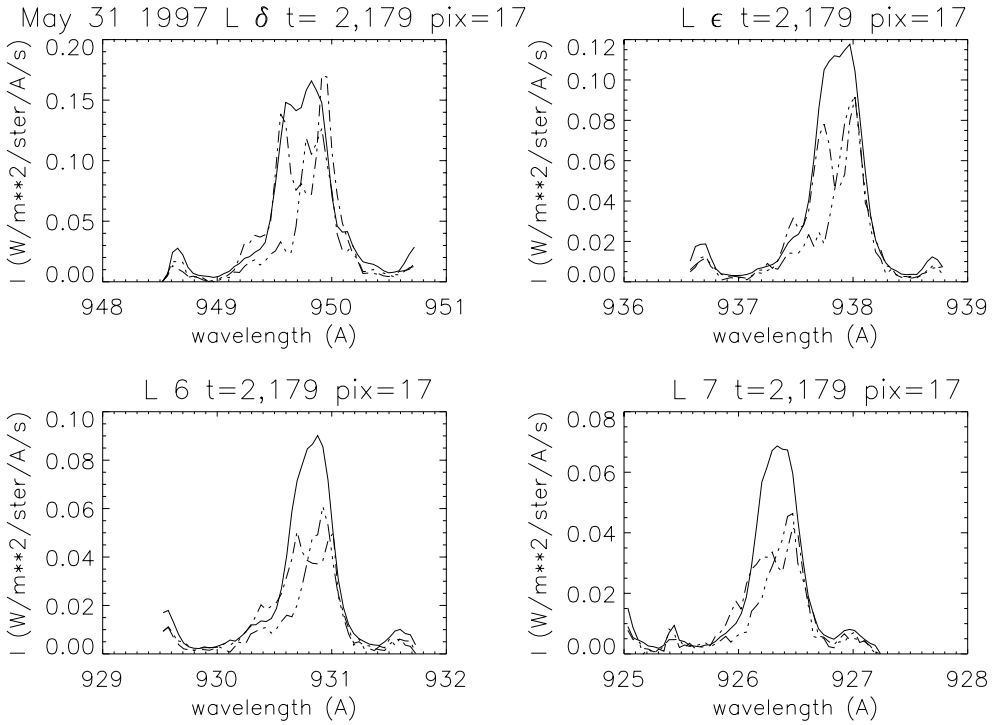

Fig. 12. Example of Lyman profiles in the filament before its eruption at 08:22 UT (dash-doted line), during eruption at 11:25 UT (3 dots dashed line), on the disk (continuous line). Pixel 17 corresponds to the location indicated by the arrow in Fig. 11.

vations are supported by the sketch proposed by Raadu et al. (1988). The observations show that the filament is in a dynamic configuration. The dynamics is evident in terms of large scale mass motions of the sections of the filament and in terms of microturbulence. The upward motion should lead to a rise of the filament, and an expansion of the flux tubes containing the filament material since the surrounding pressure is decreasing with height. Conservation of the current and the magnetic flux along the filament then requires twisting motions as the flux rope adjusts to a new radial equilibrium as it rises in the corona. The destabilization of the filament could be explained by reconnection process in a 3D magnetic configuration as proposed new generation models where lateral footpoints are due to the presence of parasitic polarities (Aulanier et al. 1999). The signature of the reconnection would be the X-ray bright point.

Consequently LASCO observed a CME. The onset of the CME is already visible in EIT 304 Å images with the lift up of long stretched field lines of the footpoint F. The velocity of the threads (SUMER-Lyman line Dopplershifts) is around 70 km s^{-1} at 11:20 UT, velocity of the same order as the bright loop, front edge of the CME visible in LASCO C2 at 12:13 UT. A deviation of the $H\alpha$ filament and the LASCO bright loop towards the equator is observed during the pre eruption and the CME evolution, constraining the event to follow the equatorial streamer field lines. The eruption and the CME are well, spatially and temporally, related showing that they belong to the same event, the same magnetic instability.

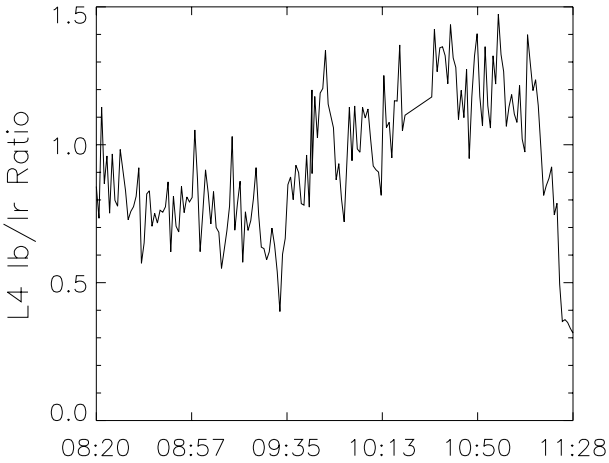

Fig. 13. Ratio Ib/Ir between the two peaks the blue (Ib) and the red peak (Ir) of Lyman line L4 versus time. Symmetric profiles correspond to a ratio equal to 1. Low ratio corresponds to missing blue peak profiles.

Acknowledgements. The SUMER project is financially supported by DLR, CNES, NASA and PRODEX. SUMER is part of SOHO the Solar and Heliospheric Observatory of ESA and NASA. These observations have been obtained during a MEDOC (Orsay) campaign. The MSDP data were reduced at the MAMA densitometer of the Observatory of Paris. We would like to thank Drs. Mein N. and Mein P. to have helped us in the MSDP data reduction and Dr P. Heinzel for fruitful discussions on the application of the cloud model method. Y.D. wants to thank the CNRS and Chinese Academy for the financial support of his stay at the Observatoire de Meudon in the context of a french-chinese bilateral program. M.M. was supported by PECO-CEI Program 5134.

References

Antiochos S.K., DeVore C.R., Klimchuk J.A., 1999, ApJ 510, 495
Aulanier G., Démoulin P., 1998, A&A 329, 125
Aulanier G., Démoulin P., Mein N., et al., 1999, A&A 342, 867
Brueckner G.E., Howard R.A., Koomen M.J., Korendyke C.M., Michels D.J., 1995, Solar Phys. 162, 357

D'Azambuja L., 1948, Thesis at the Observatory of Paris
Delaboudinière J.-P., Artzner G.E., Brunaud J., et al., 1995, Solar Phys. 162, 291
Delannée C., Aulanier G., 2000, Solar Phys., in press
Delannée C., 2000, Journal of Atmospheric and Solar-Terrestrial Physics, in press
Démoulin P., Vial J.C., 1992, Solar Phys. 141, 289
Dere K.P., Brueckner G.E., Howard R.A., Michels D.J., Delaboudinière J.P., 1999 ApJ 516, 465
Harrison R.A., Sawyer E.C., Carter M.K., et al., 1995, Solar Phys. 162, 233
Kuin P., Martens P., 1986, In: Poland A. (ed.) CPP workshop proceedings, NASA 2442, p. 241
Mein P., 1991, A&A 248, 669
Mein N., Heinzel P., Mein P., Vial J.C., 1996, A&A 309, 275
Mouradian Z., Martres M.J., Soru-Escaut I., 1986, In: Poland A. (ed.) CPP workshop proceedings, NASA 2442, p. 221
Raadu M., Malherbe J.-M., Mein P., Schmieder B., 1987, Solar Phys. 109, 59
Raadu M., Schmieder B., Mein N., Gesztelyi L., 1988, A&A 197, 289
Schmieder B., Raadu M., Malherbe J.M., 1985, A&A 142, 249
Schmieder B., Heinzel H., Kucera T., Vial J.C., 1998, Solar Phys. 181, 309
Simon G., Mein N., Mein P., Gesztelyi L., 1984, Solar Phys. 93, 325
Simon G., Gesztelyi L., Schmieder B., Mein N., 1986, In: Proceedings: Coronal prominence Plasma. Berkley workshop
Wilhelm K., Lemaire P., Curdt E., et al., 1997, Solar Phys. 170, 75
Wood B.E., Karovska M., Chen J., et al., 1999, ApJ 512, 484